Optics & Laser Technology 166 (2023) 109593

Contents lists available at ScienceDirect

Optics and Laser Technology

journal homepage: www.elsevier.com/locate/optlastec

Full length article

Resonant amplification of slow surface plasmon polaritons in a DC current pumped semiconductor/graphene waveguide with a groove defect

I.O. Zolotovskii [a], Y.S. Dadoenkova [b], F.F.L. Bentivegna [b], A.S. Kadochkin [a], S.G. Moiseev [a,c], V.V. Svetukhin [d]

[a] Ulyanovsk State University, L. Tolstoy Str. 42, 432970 Ulyanovsk, Russia
[b] Lab-STICC (UMR 6285), CNRS, ENIB, 29238 Brest Cedex 3, France
[c] Kotelnikov Institute of Radio Engineering and Electronics of the Russian Academy of Sciences, Ulyanovsk Branch, Goncharov Str. 48, 432071 Ulyanovsk, Russia
[d] Scientific Manufacturing Complex 'Technological Centre', Shokina Sq. 1, 124498 Zelenograd, Moscow, Russia

ARTICLE INFO

Keywords:
Graphene
Surface plasmon polaritons
Electric current pump
Amplification

ABSTRACT

We propose the principle of a planar surface plasmon polariton amplifier composed of a complex waveguide structure based on a semiconductor thin film separated from a dielectric substrate by a graphene monolayer. The amplification of surface plasmon polaritons in that waveguide in the terahertz regime is driven by a direct current in the graphene layer under a synchronism condition that allows an efficient energy exchange from the collective flux of charge carriers in graphene and the surface electromagnetic wave in the semiconductor film. Positive feedback required for resonant amplification is achieved through surface plasmon polariton reflections at the edges of the active waveguide, one of which is formed by a local thickness defect (a groove) at the upper surface of the semiconductor film that also provides an exit channel for the energy of the amplified surface wave to be transferred to an adjacent passive thin film semiconductor waveguide. We determine the conditions required for the resonant amplification of surface plasmon polaritons in that complex structure, which are essentially governed by the geometry of the groove as well as by the characteristic parameters of the active and passive waveguides.

1. Introduction

Surface plasmon polaritons (SPPs) are localized electromagnetic waves coupled with the density fluctuations of free charge carriers at the interface between two materials with respectively positive and negative dielectric permittivities (typically, a dielectric and a metal) or in one- or two-dimensional conducting materials (carbon nanotubes, graphene, borophene, etc.) A major drive towards the use of plasmonic fields instead of optical ones is that the former make it possible to achieve noticeable progress in the miniaturization of devices because of their extreme spatial localization. Recently, a great variety of plasmonic devices have been proposed and studied, including plasmonic lasers, waveguides, switches, absorbers, plasmonic nanosensors and metasensors [1–8]. To mention but a few recent and prominent examples, a plasmonic ultra-broadband terahertz absorber has been realized in a graphene metamaterial [9], and the enhancement of light-matter interactions at THz frequencies has been obtained by plasmonic excitations in graphene nanostructures [10,11]. THz plasmonics have also been shown to be very promising, in particular for next-generation wireless communication [12] and biosensing techniques [13].

One of the many directions of research in the field of plasmonics is devoted to plasmonic waveguides. Because of the high confinement of electromagnetic energy they provide, beyond the diffraction limit of light, SPPs propagating in a guiding structure represent a promising way towards next-generation circuits in which light can be used to overcome the speed limit of electronics. Various types of plasmonic waveguides have been proposed in recent years, including metallic films, grooves, strips, and wedges, metal/insulator/metal slabs, nanowires and chains of nanoparticles [2]. On the basis of such waveguides, nearly all the basic digital components analogous to the traditional electronic devices composing a complex functional circuit have been developed, including plasmonic lasers, plasmonic modulators, logical gates, switches, routers, photon-electric converters or Mach–Zehnder interferometers [14].

However, the development of plasmonic devices is hampered by the strong ohmic losses of SPPs upon propagation, which calls for the design of efficient amplification methods. In that context, the possibility of compensating losses by introducing optical gain in the plasmonic system has been actively investigated since the late 1970s [15,16]. The

E-mail address: rafzol.14@mail.ru (I.O. Zolotovskii).

https://doi.org/10.1016/j.optlastec.2023.109593
Received 13 January 2023; Received in revised form 10 April 2023; Accepted 10 May 2023
Available online 2 June 2023

amplification of SPPs was experimentally demonstrated, for example in metallic nanofilms combined with optically pumped gain media [17,18], or by electrical injection in hybrid plasmonic waveguides [19,20]. Recent experimental and theoretical studies have also demonstrated that under optical excitation graphene layers can exhibit a negative dynamic THz conductivity associated with population inversion and the domination of interband emission over intraband Drude absorption [21,22]. This was proposed to be used for the design of SPP amplifiers and lasers operating in the THz domain [22–25]. In recent years, an alternative SPP amplification mechanism has been proposed that involves the transfer of kinetic energy, from the collective flow of free electrons in a graphene layer adjacent to a plasmonic waveguide, to the surface electromagnetic wave the waveguide supports [26–31]. This mechanism does not involve any active medium in which population inversion needs to be achieved through pumping, and the systems that exploit it behave as optical amplifiers for SPPs co-propagating with the drifting electrons and as strong attenuators for counter-propagating SPPs. In addition, incorporating them in a cavity leads to the realization of SPP oscillators – known as SPP lasers or 'spasers'.

In this paper, we propose a method for resonant electric-current-driven amplification of SPPs in a planar resonator in a geometry such that the amplified field can be extracted from the resonator into a plasmonic waveguide, which makes it possible to use the proposed amplifying structure as part of a plasmonic generator scheme. Specifically, the proposed plasmonic device, as described in Section 2, is a complex planar structure based on a semiconductor film located atop a dielectric substrate. A graphene monolayer is inserted along part of the geometric boundary between these two materials. That region forms an active waveguide for SPPs when a DC electric current circulates in the graphene layer, so that amplification of SPPs through that current can take place under specific conditions. Section 3 shows that amplification can be made resonant, and the active waveguide thus becomes a resonator, thanks to the presence of the narrow and shallow groove at the upper surface of the semiconductor film that acts as a reflector and provides the necessary feedback. Across the groove, the semiconductor film forms an adjacent, passive waveguide that provides a convenient way to extract the amplified radiation. In previous papers [26–28], we discussed the principle of such a current-driven SPP amplification scheme, but without groove. In Ref. [26], extraction of the radiation to the free space was proposed to be achieved through a diffraction grating, which meant that the amplified radiation was not efficiently channeled out of the structure. In the present work, the presence of the groove is thus a crucial improvement to those previous studies, in that it allows a direct and efficient extraction of the amplified radiation and thus eases the integration of the structure in low-dimensional photonic devices. Furthermore, we show that the groove does not only provide an efficient way to obtain a SPP resonator and an extraction method, but, as shown by numerical results in Section 3, it also governs, through the careful choice of its length and depth, (along with the geometrical and constitutive parameters of the active waveguide itself) the electric-current-mediated SPP amplification efficiency and energy extraction efficiency of the whole structure.

2. Description of the structure and dispersion relations of surface plasmon polaritons

We consider a complex structure formed by two planar waveguides (whose guiding layers are made of the same semiconductor medium B) separated by a defect layer, also made of medium B, with a rectangular groove on its top surface (Fig. 1). These semiconducting layers are deposited atop a dielectric substrate (medium C) and surmounted by a dielectric medium (medium A). In the whole paper, parameters related to the left-hand-side waveguide, the groove, and the right-hand-side waveguide will be referred to with indices 1, 2, and 3, respectively.

We assume that SPPs of angular frequency ω in the far-infrared domain propagate along the boundary between medium B and substrate C along the x-axis of a (xyz) Cartesian system of coordinates in which that boundary is parallel to the (xy) plane. In this paper, the time dependence of the electromagnetic fields will be taken as $\exp(i\omega t)$.

In the spectral domain of interest, materials A and C are transparent,

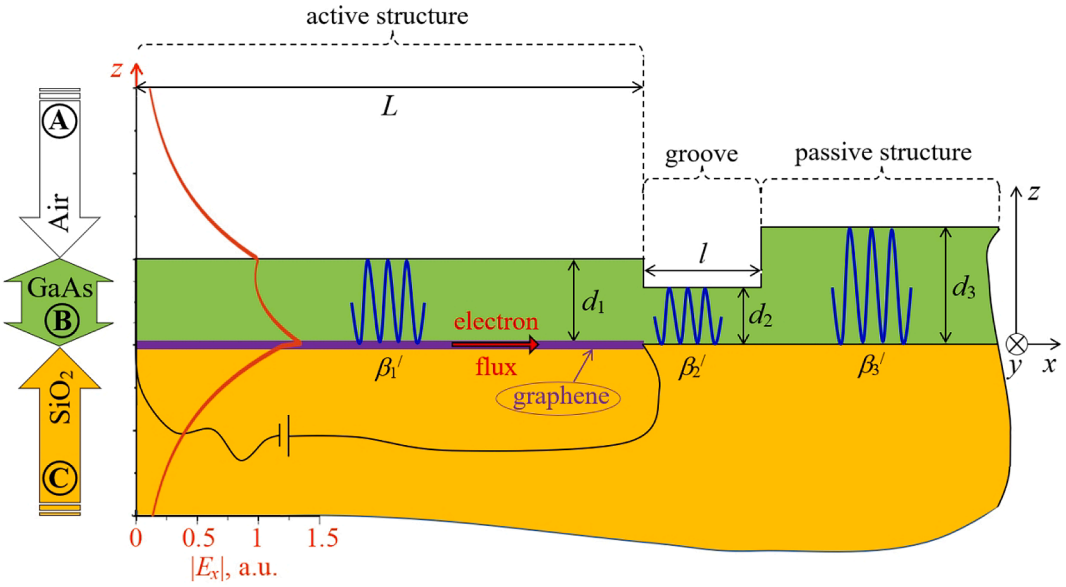

Fig. 1. Schematic of a SPP amplifier with radiation propagation into a planar waveguide. An active plasmon waveguide of length L (with a graphene monolayer located between a semiconductor film of thickness d_1 and a dielectric substrate) is adjacent to a passive waveguide made of a semiconductor film of thickness d_3 deposited on the dielectric substrate. The active and passive guiding layers are separated by a rectangular groove of length l located atop a semiconductor layer of thickness d_2. The active and passive waveguides and the groove region are all made of the same semiconductor B. Materials A and C are the dielectric surrounding medium and the substrate. The propagation constants of the SPPs in the active waveguide, groove region and passive waveguide are denoted β'_1, β'_2, and β'_3, respectively. The electron flux driven by a DC applied voltage in the active structure is directed along the positive direction of the x-axis. The red curve represents the distribution along the z-axis of the absolute value of the longitudinal electric field component $|E_x|$ of the SPP field in the substrate, waveguide and superstrate of the active region.

with real relative dielectric permittivities $\varepsilon_A > 0$ and $\varepsilon_C > 0$, respectively, whereas semiconducting material B is partially absorbing, with, for the chosen time dependence for the fields of propagating SPPs, negative real and imaginary parts ($\varepsilon_B^{'} < 0$ and $\varepsilon_B^{''} < 0$) of its complex relative dielectric permittivity defined as $\varepsilon_B = \varepsilon_B^{'} + i\varepsilon_B^{''}$. In the following, numerical calculations will be carried out for air (surrounding medium A), gallium arsenide GaAs (semiconductor B) and silicon SiO_2 (substrate C).

In the (xyz) system of coordinates, the left-hand-side boundary of the first planar waveguide separates surrounding medium A and semiconductor B and is located at $\times = 0$. The length of this waveguide along the x-axis is L. Over its whole length, the lower boundary of the waveguide separating medium B from substrate C is covered with a graphene layer, which provides a means to amplify SPPs propagating along the x-axis through energy exchange between the SPPs and a DC current injected in graphene (see below for a description of the amplification mechanism), so that the waveguide can be considered as an active structure. Its right-hand side boundary, at $\times = L$, is bordered by a shallow groove of length l in the semiconductor film B that constitutes the defect mentioned above. This groove provides a partial reflection of SPPs into the first waveguide. The fraction of a SPP crossing the groove propagates further in the second, passive waveguide. The guiding layers of the active and passive waveguides have thicknesses d_1 and d_3, respectively. The groove region can also be considered as a passive waveguide of length l and thickness d_2 (with $d_2 < d_1$, d_3).

The electric field components of SPPs propagating along the boundary can be written as $\widetilde{E}_j(x,z,t) = E_j(x,z)\exp[i(\omega t \pm \beta_j x)]$ with $j = 1$, 2, 3, where complex SPP wavevector amplitudes $\beta_j = \beta_j^{'} + i\beta_j^{''}$ refer to the active waveguide ($j = 1$, for $0 \le x \le L$), the groove region ($j = 2$, for $L < x < L + l$) and the passive waveguide ($j = 3$, for $\times \ge L + l$), respectively. The sign '–' (resp. '+') in the phase of $\widetilde{E}_j(x,z,t)$ corresponds to SPPs propagating along the positive (resp. negative) direction of the x-axis. The propagation of SPPs in both directions is due to scattering at the boundaries of the groove as well as reflection on the left-hand side edge of the active waveguide. Back reflection from the right-hand side of the passive waveguide is neglected.

The mechanism of SPP amplification in the active waveguide is based on the direct energy transfer, through the Cherenkov effect, from the flux of moving charge carriers forming the electric current in the graphene layer to the surface-localized electromagnetic wave in the semiconducting layer [26]. The same physical principle is used in the traveling-wave tubes well known in microwave technology [32]. A crucial condition to the achievement of an effective interaction and energy exchange between the SPP and the direct electric current is to equate the phase velocity of the electromagnetic wave to the drift velocity of the electric current. Thus, it is essential to determine the optimal characteristic parameters of the plasmonic structure for which this synchronism condition is satisfied.

This amplification mechanism is neither directly related to the characteristic properties of the materials in the structure, nor does it affect them (in contrast to the amplification due to pumping mechanisms in laser media, for instance). This makes it possible to analyze the dispersion relation dependences $\beta_j(\omega)$ using results known for SPPs in layered structures composed of passive (non-amplifying) media. Thus, in the active waveguide, provided that $d_1 \ll L$, the dispersion relation of a SPP propagating along either the positive or the negative directions of the x-axis in the semiconductor layer takes the form [33]

$$\exp(-2q_{1B}d_1) = \frac{q_{1B}\,\varepsilon_A + q_{1A}\,\varepsilon_B}{q_{1B}\,\varepsilon_A - q_{1A}\,\varepsilon_B}\cdot\frac{(q_{1B}\,\varepsilon_C + q_{1C}\,\varepsilon_B)\varepsilon_0\omega + iq_{1B}\,q_{1C}\,\sigma}{(q_{1B}\,\varepsilon_C - q_{1C}\,\varepsilon_B)\varepsilon_0\omega + iq_{1B}\,q_{1C}\,\sigma} \tag{1}$$

where $q_{1\kappa} = \sqrt{\beta_1^2 - k_0^2\varepsilon_\kappa}$ is the z-component of the complex SPP wavevector in the medium with dielectric permittivity ε_κ ($\kappa = A,B,C$), σ is the surface conductivity of graphene, ε_0 is the vacuum permittivity, and $k_0 = \omega/c$ and c are the wavevector modulus and speed of light in vacuum, respectively. For both the groove region (semiconductor layer thickness d_2) and the passive waveguide (semiconductor layer thickness d_3) the dispersion equations of a SPP write

$$\exp(-2q_{jB}d_j) = \frac{q_{jB}\varepsilon_A + q_{jA}\varepsilon_B}{q_{jB}\varepsilon_A - q_{jA}\varepsilon_B}\cdot\frac{q_{jB}\varepsilon_C + q_{jC}\varepsilon_B}{q_{jB}\varepsilon_C - q_{jC}\varepsilon_B}, \qquad j = 2,\ 3 \tag{2}$$

where $q_{j\kappa} = \sqrt{\beta_j^2 - k_0^2\varepsilon_\kappa}$ is again the z-component of the complex SPP wavevector in the medium with dielectric permittivity ε_κ ($\kappa = A,B,C$) and j refers to the groove region ($j = 2$) or the passive waveguide ($j = 3$).

Here it must be emphasized that localized SPPs are present at both interfaces (*i.e.*, at the superstrate/semiconductor A/B interface as well as at the semiconductor/substrate B/C interface), as schematically illustrated in Fig. 1 by the distribution of the longitudinal electric field component $|E_x|$ of the SPP field along the z-axis (see the red curve). Here, the field is represented in arbitrary units and normalized to 1 at the A/B interface. For an asymmetric structure such as that under study, in which the surrounding medium A and the substrate C have very different permittivities, SPP localization is stronger at one of the interfaces (here, at the B/C interface, thus justifying the principle of energy exchange between the dc current and the propagating SPPs), but the SPP amplitude along the other interface is non-zero and cannot be neglected. This is reflected in Eqs. (1) and (2), in which the dielectric permittivities of all three media, as well as the surface electric conductivity of graphene, intervene. In Fig. 1, SPP propagation has schematically been shown to occupy the whole thickness of the semiconductor film for the sake of readability. Note that the distribution of $|E_x|$ exhibits the same evolution in the groove region and in the passive structure.

In the frequency range considered in the present study (4.67 THz ± 5 GHz) the chromatic dispersion of dielectric permittivities of the surrounding medium ε_A and of the substrate ε_C can be neglected, with $\varepsilon_A = 1$ (air) and $\varepsilon_C \approx 4$ (SiO_2) [34], respectively. The spectral variations of complex permittivity ε_B in a semiconductor crystal such as GaAs, on the other hand, cannot be neglected and are taken to obey the following dependence [35]:

$$\varepsilon = \varepsilon_\infty\left(1 + \frac{\omega_{LO}^2 - \omega_{TO}^2}{\omega_{TO}^2 - \omega^2 + i\omega\gamma} - \frac{\omega_p^2}{\omega(\omega - i\gamma_D)}\right) \tag{3}$$

where ε_∞ is the relative permittivity in the high-frequency limit (optical frequencies), ω_{TO} and ω_{LO} are the angular frequencies of the transverse and longitudinal optical phonons in the crystal, γ_{ph} is the phonon damping constant, and γ_p is the plasmon damping constant (the free-carrier damping constant). The plasma angular frequency $\omega_p = \sqrt{nq_e^2/(m^*\varepsilon_\infty\varepsilon_0)}$ depends in particular on the volume density n, the charge q_e, and the effective mass m^* of the free electrons in GaAs. The second term on the right-hand side of Eq. (3) describes the interaction of the electromagnetic field of the SPP with optical phonons in the semiconductor in the frame of the Lorenz model, whereas the third term describes the interaction of that field with the free carriers in the frame of the Drude model.

Finally, the surface conductivity of graphene in Eq. (1) is calculated using the following expression, in which losses are taken into account [36]:

$$\sigma(\omega,\mu_c,\Gamma,T) = \frac{ie^2(\omega + i2\Gamma)}{\pi\hbar}\left[\int_0^\infty \frac{f_d(-\omega) - f_d(\omega)}{(\omega + i2\Gamma)^2 - 4\omega^2}\,d\omega - \frac{1}{(\omega + i2\Gamma)^2}\int_{-\infty}^{\infty}\frac{\partial f_d(\omega)}{\partial\omega}\,|\omega|\,d\omega\right] \tag{4}$$

where Γ is the phenomenological scattering rate of electrons in the graphene layer and $f_d = \{\exp[(\hbar\omega - \mu_c)/k_BT] + 1\}^{-1}$ is the Fermi-Dirac distribution, in which μ_c is the chemical potential of electrons in graphene, T is the temperature, $\hbar$ is the reduced Planck constant, and k_B is

the Boltzmann constant.

Material parameters of GaAs and graphene used for the numerical calculations are gathered in Table 1.

It should be noted that, as can be expected from Eq. (1), the complex wavevector amplitude $\beta_1 = \beta_1' + i\beta_1''$ of the SPP in the active waveguide, and thus its phase velocity $V_1 = \omega/\beta_1'$, depend on the thickness d_1 of the semiconductor layer. Thus, the SPP frequency, at which the synchronism condition between the surface electromagnetic wave and the current carriers flowing in the graphene monolayer is met, can be adjusted by varying d_1. The choice made in our study for both the constituting materials and the dimensions of the structure ensures that in the vicinity of SPP frequency $\nu = 4.67$ THz (*i.e.,* for angular frequency $\omega \approx 29.3 \cdot 10^{12}$ rad•s^{-1}), the propagation constant of a SPP in the active plasmonic waveguide is two orders of magnitude larger than the wavevector modulus of light in vacuum ($k_0 \sim 10^5$ rad•m^{-1}). As a consequence, the phase velocity V_1 of a SPP in that waveguide is about two orders of magnitude smaller than the speed of light in vacuum ($c \approx 3 \cdot 10^8$ m·s^{-1}), and can be equal to, and even smaller than the drift velocity of charge carriers in graphene $V_{gr} \approx 0.8 \cdot 10^6$ m·s^{-1} [38], which ensures that the synchronism condition mentioned above can be fulfilled.

As is well known, the electric properties of graphene are related to its Fermi energy (chemical potential at room temperature), and they can be tuned by changing the charge concentration, which can be realized by external or internal means, for instance chemical doping, the nature of the substrates, applied electric or magnetic fields, and even temperature [2]. Thus, any change in the characteristics of graphene, including the level of its doping, leads to a change in the spectral behavior of the SPPs and, as a consequence, to a change in the spectral frequency band in which SPPs can be amplified by the pump current. However, numerical analysis shows that for the parameters adopted in this study, the propagation constants of the SPPs are mainly determined by the parameters of the semiconductor waveguiding film, and that the influence of graphene on β_1' can in first approximation be neglected.

3. Resonant amplification of surface plasmon polaritons driven by a DC current in the graphene layer

The structure under consideration (Fig. 1) is an analog of a resonant active Fabry-Perot cavity, in which the resonator consists of the active waveguide and of its facets that act as reflectors and provide the positive feedback necessary for the establishment of a regime of generation of SPPs. The transmission and reflection characteristics of the right-hand-side reflector are defined by the structural parameters of the groove region. In this Section, we discuss the conditions of a resonant amplification of SPPs in such a structure (a necessary condition for SPP generation) when a DC electric current flows in the graphene layer.

Table 1
Material parameters of GaAs and graphene used for numerical calculations.

Material	Parameters
Semiconductor GaAs [35]	$\varepsilon_\infty = 11$
	$\omega_{TO} = 50.5 \cdot 10^{12}$ rad·s^{-1}
	$\omega_{LO} = 55 \cdot 10^{12}$ rad·s^{-1}
	$\gamma_{ph} = 0.45 \cdot 10^{12}$ s^{-1}
	$\gamma_p = 2.33 \cdot 10^{12}$ s^{-1}
	$m^* = 0.071\ m_e$ ($m_e = 9.1{\cdot}10^{-31}$ kg is the electron rest mass)
	$q_e = -1.6{\cdot}10^{-19}$C
	$n = 35{\cdot}10^{22}$ m^{-3}
Graphene [37–39]	$T = 300$ K
	$\mu_c = 0.2$ eV
	$\hbar\Gamma = 1$ meV

3.1. Single-pass amplification in the active waveguide

Let us first describe SPP amplification in a single-pass regime in the active waveguide itself before discussing resonant amplification in Subsection 3.2.

The energy transfer from the direct current to a SPP can be described within the frame of Pierce's classical theory of traveling-wave tubes, familiar in microwave technology, that describes the generation of coherent radiation from the interaction of an electron beam with a microwave beam in a waveguide. As mentioned above, the amplification of the electromagnetic wave requires a match of its phase velocity with the drift velocity of the charge carriers. For the structure under consideration here, fulfilling that condition for the electromagnetic component of a SPP and the electrons flowing in the graphene layer ensures an effective transfer of energy from the DC current to the surface electromagnetic wave. Following Pierce's approach, the expression can be derived for the dispersion relation of a SPP interacting with a flow of electrons propagating in the same direction with the drift velocity V_{gr} [26–28]:

$$(\omega - G\,V_1)(\omega - G\,V_{gr})^{\,2} = C\,\omega^{\,3} \tag{5}$$

where G is the complex variation rate of the harmonic field amplitude of the SPP, and the Pierce parameter C can be written as

$$C \approx \frac{\omega_q^2}{2\varepsilon_\infty(\omega^{\,2} + \omega_p^2)} \frac{(\varepsilon_B'\,k_0)^2}{\beta_1'^2(\varepsilon_B' + \varepsilon_C)^2 + (\varepsilon_B' k_0)^2} \frac{V_1}{V_{g_1}} \tag{6}$$

In Eq. (6), $V_{g_1} = \partial\omega/\partial\beta_1'$ is the group velocity of the SPPs in the active waveguide, and $\omega_q = \sqrt{n_{gr}\,q_{gr}^2\,\beta_1'/(m_{gr}\,\varepsilon_0)}$ is the plasma angular frequency in graphene, where q_{gr}, m_{gr}, and n_{gr} are the charge, effective mass and surface density of charge carriers in graphene, respectively. For the numerical calculations, we take $q_{gr} = q_e$, $m_{gr} = m_e$, and $n_{gr} = 10^{16}$ m^{-2} [40]. In our system, the SPP group velocity is about $V_{g_1} = 0.7{\bullet}10^6$ m·s^{-1}.

Given the choice of time dependence we made for the SPP fields, the spatial dependence of the electric field of a SPP propagating in the positive direction of the x-axis (*i.e.*, codirectionally to the electron flux in graphene, as required by the amplification mechanism) is $\widetilde{E}_x \sim \exp[-iGx)]$, and the only root of the third-degree polynomial in Eq. (5) solved for G that can yield the value of the SPP field amplification coefficient α is a complex root whose imaginary part is such that $\alpha = Im(G) \geqslant 0$.

Fig. 2 shows the results of the numerical determination of the effective single-pass amplification coefficient $\alpha - |\beta_1''|$, which takes into account the loss coefficient $|\beta_1''|$ in the active waveguide as a function of the SPP frequency for semiconductor film thickness $d_1 = 50$ nm. The spectral dispersion of the loss coefficient in the considered waveguide is very small in the frequency range under consideration, where the average value of $|\beta_1''|$ is about $0.0347{\cdot}10^5$ m^{-1}. For that value of the loss coefficient, the SPP propagation length is about 144 μm, *i.e.*, about 2.25 times the vacuum SPP wavelength in the frequency range under consideration, which is in agreement with values reported in various semiconducting plasmonic structures in the far-infrared frequency range [41,42]. A frequency range exists (green area) for which α can reach large values that exceed $|\beta_1''|$, which means that a SPP propagating codirectionally to the electron flux in graphene is amplified along the length of the active waveguide. For the structural and constitutive parameters chosen in this work, that range lies in the THz domain, centered around 4.671 THz, with a narrow width of about 6.98 GHz.

As was mentioned above, the spectral range for which a SPP can be amplified is determined by the ratio of the drift velocity V_{gr} of the current carriers in graphene and the phase velocity V_1 of the SPP, and the latter is in particular a function of the thickness d_1 of the semiconductor film in the active waveguide, as indicated by Eq. (1). It should be noted that, all other parameters being equal, calculations show that no SPP

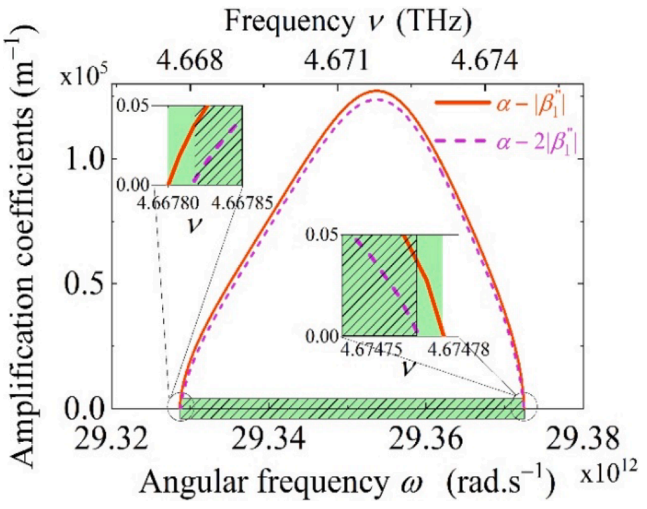

Fig. 2. Spectra of the effective SPP single-pass amplification coefficient $\alpha - |\beta_1''|$ (orange line) and effective SPP resonant amplification coefficient $\alpha - 2|\beta_1''|$ (violet line) in the active waveguide. The green area corresponds to the frequency range where the single-pass amplification condition $\alpha > |\beta_1''|$ is satisfied, and the shaded area shows the resonant amplification condition $\alpha > 2|\beta_1''|$. The insets zoom in on the low- and high-frequency borders of the amplification ranges. Calculations were carried out for semiconductor film thickness $d_1 = 50$ nm.

amplification can take place for d_1 larger than approximately 60 nm, in which case the SPP phase velocity takes higher values and therefore the synchronism cannot be fulfilled. However, even for such thin films, the synchronism condition can still be met by increasing the drift velocity V_{gr}, for example *via* Fermi velocity engineering techniques [43,44]. This opens up additional opportunities for the amplification of SPPs which, however, are beyond the scope of this article.

It should be noted that in practice, deviations of the film thickness may occur, for instance due to imperfections of the film growth or to surface roughness, which can affect the amplification regime of the SPPs via i) a change of the amplification coefficient; ii) an increase of the losses. Our calculations show that a 10% increase (resp., decrease) of the semiconductor film thickness d_1 leads to a slight shift of about 0.6 GHz of the amplification band towards higher (resp., lower) frequencies, together with an approximately 15% increase (resp., decrease) of the SPP amplification coefficient. Thus, the amplification coefficient remains of the same order of magnitude, which is expected to compensate for the increased losses arising from surface roughness.

3.2. Amplification of SPPs in the resonator

The active waveguide structure shown in Fig. 1 is limited along the *x*-axis by two reflectors on which propagating SPPs undergo (partial) reflection, and it can thus be seen as a *resonator*. On its left-hand side, the reflector consists of an interface between the semiconductor layer B and the surrounding medium A. On its right-hand side, partial reflection occurs at each extremity of the groove region, and the latter can be seen as a distributed reflector. As a result, standing SPP waves are formed in the active structure. As in a laser cavity, SPP generation is conditioned by the reproduction of the complex wave amplitude upon a complete roundtrip in the resonator [45]. Taking into account the fact that amplification can be achieved in one direction only (in the direction of the electron flux in graphene), the SPP resonant amplification condition reads

$$\rho_{left}\,\rho_{right}\exp\left[\left(\alpha + 2\beta_1''\right)L\right]\exp\left[-2i\beta_1' L\right] = \exp\left[-2i\pi m\right] \tag{7}$$

where m is a positive integer, and ρ_{left} and ρ_{right} are the reflection coefficients of the left-hand- and right-hand-side reflectors, respectively. As follows from Eq. (7), the frequency domain over which generation of SPPs is possible is restricted by the condition $\alpha > 2|\beta_1''|$ (shown by the shaded area in Fig. 2). This region is thus narrower than the single-pass amplification bandwidth resulting from the $\alpha > |\beta_1''|$ amplification condition of a SPP by a DC electric current pumping in graphene (shown by the green area in Fig. 2). However, the difference between these frequency ranges remains small due to the very large value of the amplification factor. For instance, for a semiconductor film thickness $d_1 = 50$ nm in the active waveguide, the spectral dependencies of α and β_1'' yield a resonant amplification band $\Delta\nu_{res} = (4.66782 - 4.674776)$ THz, which is slightly narrower than the single-pass amplification band $\Delta\nu = (4.66780 - 4.67478)$ THz.

In the most general case, discontinuities related to irregularities in the plasmonic waveguide lead to the parasitic scattering of SPPs both inside the waveguide and outside, *i.e.*, into the superstrate and the substrate. The complete description of the behavior of SPPs at discontinuities requires complex three-dimensional numerical methods. However, analytical and semi-analytical methods are still applicable in many plasmonic systems in which parasitic scattering can be neglected [46–51]. Thus, in this paper, the calculation of the reflection coefficient at the boundaries of the groove region is carried out using Fresnel-like relations. This analytical method provides good approximations provided the variation in SPP effective refractive indices β_i/k_0 across the groove boundaries remains small [46,52,53]. Small differences between propagation constants β_1, β_2 and β_3 are achieved for small differences between film thickness d_1, d_2 and d_3, and the overall complex reflection coefficient, for SPP field amplitudes, of the groove seen as the distributed right-hand-side reflector of the cavity can be written using Airy's formula:

$$\rho_{right} = \frac{r_{12} + r_{23}\exp[-i2\beta_2 l]}{1 + r_{12}\, r_{23}\exp[-i2\beta_2 l]} \tag{8}$$

where

$$r_{\eta\,\zeta} = \frac{\beta_\eta - \beta_\zeta}{\beta_\eta + \beta_\zeta}, \quad \{\eta, \zeta\} \in \{\{1, 2\}, \{2, 3\}\} \tag{9}$$

is the complex amplitude Fresnel-like reflection factor under normal incidence at the interface separating regions η and ζ.

For simplicity, we consider the case where the thicknesses d_1 and d_3 of the GaAs films on either side of the groove region are equal (so that $\beta_1 \approx \beta_3$, since the influence of the graphene layer on β_1 can be neglected) and, as mentioned above, do not differ much from the thickness d_2 of the GaAs film under the groove ($|d_{1,3} - d_2| << d_{1,2,3}$). Equation (8) then takes the following simplified form:

$$\rho_{right} \approx \frac{\beta_1 - \beta_2}{\beta_1 + \beta_2}\left(1 - \exp[-i2\beta_2 l]\right) \tag{10}$$

Equation (10) shows that the reflection of SPPs due to the presence of the groove is in particular governed by the mismatch between the propagation constants in regions 1 (active waveguide) and 2 (under the groove of depth $d_1 - d_2$). The reflection coefficient ρ_{right} also exhibits an oscillating dependence on the groove length l. As a result, it is possible to tailor the characteristics of the resonant cavity inside which SPPs can be generated and amplified through the choice of the geometric dimensions of the groove. It must be noted, however, that such a modulation of the reflection coefficient of the distributed reflector is only realistically feasible for a limited range of groove length l, since dissipative losses across the groove increase exponentially with l (with SPP amplitude decaying as $\exp[2\beta_2'' l]$), so that for large values of l, the SPP is for all intents and purposes extinguished before reaching the passive waveguide.

The left-hand-side facet of the active waveguide exhibits an abrupt refractive index transition. Strongly localized SPPs are known to expe-

rience near total reflection at such boundaries [54,55], and the corresponding reflection coefficient can thus be written as

$$\rho_{left} \approx \exp(i\Theta) \tag{11}$$

where Θ is the phase shift upon reflection, which in plasmonic structures can take values in the entire range [0, 2π] [55–59].

Substituting Eqs. (10) and (11) into Eq. (7) and noting that for the choice we made for the time dependence of the fields and the definition of the complex propagation constants, losses in all regions are associated to $\beta_i'' < 0, \quad i \in \{1, 2, 3\}$, we obtain the following condition for the resonant amplification of SPPs in the active waveguide:

$$\frac{\beta_1 - \beta_2}{\beta_1 + \beta_2}\left(1 - \exp\left[2\beta_2'' \quad l\right]\exp\left[-i\ 2\beta_2'\ l\right]\right)\exp\left[\left(\alpha + 2\beta_1''\ \right)L\right] = \exp\left[i\left(2\beta_1' L - \Theta - 2\pi m\right)\right] \tag{12}$$

Equation (12) highlights the dependence of that resonant amplification condition upon the dimensions of both the active waveguide (thickness d_1) and the groove region (length l and semiconductor film thickness d_2 under the groove). Note that d_1 and d_2 are implicitly included in Eq. (12) *via* the complex SPP wavevectors β_1 (ω_1, d_1) and β_2 (ω_2, d_2), which are determined by Eqs. (1) and (2). It should also be noted that resonant amplification is a necessary condition for the establishment of a lasing process (and as a consequence, the structure under study here would be suitable for the design of a spaser with a distributed feedback geometry), which means that Eq. (12) also expresses one condition that needs to be fulfilled in order to generate slow SPPs in the active waveguide. Thus, in the following, we will refer to Eq. (12) as the generation condition.

3.3. Numerical results and discussion

Let us now analyze Eq. (12) and study the dependence of the generation condition upon two crucial geometrical parameters of the structure — the length L of the active waveguide and the depth of the groove expressed in terms of ratio d_2/d_1.

We can first estimate the minimal value $L_{\min}(\omega)$ of the length of the resonator that allows *resonant SPP amplification at frequency ω, i. e.*, fulfills the requirement that single-pass amplification (when SPPs and DC current are co-propagating along the positive direction of the *x*-axis) exceeds losses over a roundtrip in the cavity. We neglect the term depicting energy loss in the right-hand-side distributed reflector in Eq. (12), so that $\exp[2\beta_2'' l] \approx 1$, which amounts to consider the length l of the groove to be small enough. Furthermore, we can always choose $l_n = (1 + 2n)\pi/2\beta_2'$ (where n is a positive integer) so that $\exp[-i2\beta_2' l_n] = -1$, which corresponds to a maximum of the reflectivity $|\rho_{right}|^2$ of the groove (seen as a distributed reflector) due to constructive interference (see Eq. (10)). With these assumptions, for $\alpha > 2|\beta_1''|$ we get

$$L_{\min} \approx \frac{1}{\alpha + 2\beta_1''} \ln\frac{d_1 + d_2}{2|d_1 - d_2|} \tag{13}$$

Here we used the approximation $|(\beta_1 - \beta_2)/(\beta_1 + \beta_2)| \approx |(d_1 - d_2)/(d_1 + d_2)|$, valid for SPP wavevectors greatly exceeding in modulus the wavevector modulus of light in media A, B and C, which is the case in our system.

The generation condition expressed by Eq. (12) can only be satisfied if $L \geqslant L_{\min}$, while Eq. (13) implies that $L_{\min}$ depends on the frequency of the SPP (*via* coefficients α and β_1''). The smallest value of $L_{\min}$ is logically reached at the frequency within the resonant amplification band where the effective amplification coefficient $\alpha - 2|\beta_1''|$ is maximum which, again for the parameters used in Fig. 2, takes place in the vicinity of $\omega_m = 29.353 \cdot 10^{12}$ rad·s^{-1} (where $\alpha - 2|\beta_1''| \approx 1.23 \cdot 10^5$ m^{-1}). On the other hand, Eq. (13) shows that $L_{\min}$ also depends on the respective values of the thicknesses d_1 and d_2 of GaAs in the active waveguide and under the groove. For instance, again for $d_1 = 50$ nm and for the near-optimal value $l = 60$ nm of the groove length that satisfies both $\exp[2\beta''_2 l] \approx 1$ and $\exp[-i2\beta_2' l] \approx -1$ (see the discussion above that led to Eq. (13)), the active region length must be at least 21.5 μm and 12.2 μm for a groove depth ($d_1 - d_2$) equal to 5 nm and 10 nm, respectively.

On the basis of such numerical values it appears that for any $L \geq L_{\min}$, the additional phase experienced by a SPP upon a roundtrip in the active cavity is $2\beta_1' L > 500$, which is much larger than the phase shift $\Theta \in [0, 2\pi]$ due to the reflection on its left-hand-side facet. As a consequence, the fulfillment of the generation condition expressed by Eq. (12) does not depend much on the value of Θ: indeed, for any value of Θ between 0 and 2π, the phase condition can always be satisfied by very slightly adjusting the length L of the active region, the required correction being<0.1 μm. Therefore, in the remainder of this study, we will neglect the influence of the precise value of Θ on SPP generation and amplification in the active waveguide and for simplicity, further numerical calculations will be carried out with $\Theta = 0$.

Solving Eq. (12) in order to determine the response of the structure in terms of SPP generation involves taking into account four geometrical parameters (d_1, d_2, l and L) and the frequency of the emitted SPPs. In what follows, we have restricted our discussion to the influence of three of the four geometrical parameters, setting one of them, the thickness d_1 of the waveguides, to a fixed value and playing with those describing the shape of the groove and the length of the active waveguide. Thus, solving Eq. (12) numerically allows us to estimate, within the resonant amplification band $\Delta\nu_{res}$, the acceptable depths of the groove (expressed in terms of ratio d_2/d_1 within the range $0.8 \leq d_2/d_1 < 1$) that, for given values of the length L of the active waveguide and that, l, of the groove, enable SPP generation at a given frequency. Note that values of $d_2/d_1 < 0.8$, corresponding to a deeper groove, are possible but, as mentioned above, they are more likely to give rise to the scattering of SPPs into free space that we have neglected for the sake of simplicity.

Fig. 3 shows the result of these calculations, depicting the ratio d_2/d_1 as a function of both the frequency of the generated SPP and the length of the active region, for $d_1 = 50$ nm and for two values of the length l of the groove: 10 nm and 60 nm (Fig. 3(a) and 3(b), respectively). In each case, the graph can thus be read as follows: for a given desired SPP emission frequency, a vertical cross-section of the colour plot gives a set of (d_2/d_1, L) values that permit that emission. Alternatively, for a given length L of the active waveguide, a horizontal cross-section reveals the spectral range of SPP emission and, for each frequency within that range, which value of d_2/d_1 is required to achieve it. A third way, finally, to exploit the graph is, for a given hue of the colour plot (*i.e.*, a given value of d_2/d_1), to follow the corresponding isochromatic line and thus determine the spectral range of SPP emission and which value of L is required to achieve any emission frequency in that range. Note that the region below the blue boundary of the colour plots corresponds to the generation of SPPs when the depth of the groove lies outside the domain we chose to limit ourselves to (*i.e.*, $d_2/d_1 < 0.8$).

The magenta dashed curve in both panels of Fig. 3 indicates the dependence of the minimal length $L_{\min}$ of the active region, given by Eq. (13), on the frequency of the emitted SPP for $d_2/d_1 = 0.8$. The curve does not coincide with the blue boundary of the colour plot in panel (a), because Eq. (13) was obtained for an optimal value of groove length l that satisfies the constructive interference condition (for which the reflectivity $|\rho_{right}|$ of the groove is maximal) while being small enough for losses in the groove region to be neglected. As mentioned earlier, the lowest value of l that satisfies these conditions is close to 60 nm, which is why the magenta dashed curve coincides with the blue boundary of the colour plot in the panel (b). In both panels, the angular frequency ω_m at which $L_{\min}(\omega)$ reaches its minimum is indicated by a vertical black dotted line. Comparing the colour plots in Fig. 3(a) and 3(b) shows that because $|\rho_{right}|$ nears its maximum for $l = 60$ nm, all the other parameters being equal, the spectral range for SPP generation is broader (and the required minimal length of the active region is shorter) than for

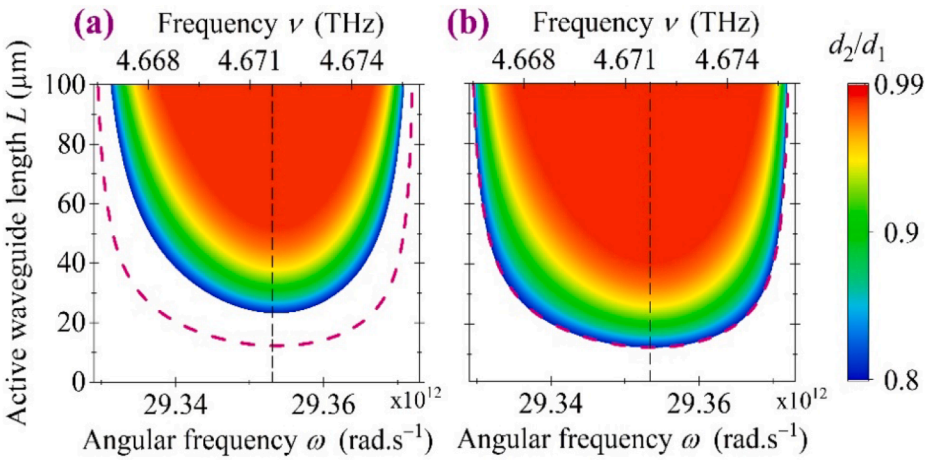

Fig. 3. Ratio d_2/d_1 calculated as a function of the frequency of emitted SPPs and the length L of the active waveguide by numerically solving Eq. (12) for waveguide thickness $d_1 = 50$ nm and for groove length l taken as (a) $l = 10$ nm and (b) $l = 60$ nm. The magenta dashed line shows the spectral dependence of the minimal value of the active waveguide length L_{min} required for SPP generation when $d_2/d_1 = 0.8$, as estimated by Eq. (13). The vertical black dashed line shows the angular frequency $\omega_m = 29.353 \cdot 10^{12}$ rad·s^{-1} for which L_{min} is smallest.

$l = 10$ nm. The value of $L_{min}(\omega_m)$ obtained through the numerical solving of Eq. (12) is approximately 12.26 μm for $l = 60$ nm, which is about 0.06 μm larger than the value 12.2 μm estimated using Eq. (13).

As a corollary to the previous discussion, Fig. 4 shows results of the numerical solving of Eq. (12), this time for fixed values of the length L of the active region ($L = 15$ μm, 20 μm, and 30 μm in panels (a), (b) and (c), respectively), thus depicting, again for $d_1 = 50$ nm, the ratio d_2/d_1 as a function of the frequency of the generated SPP and the groove length l.

Domains of potential SPP generation are repeated periodically as l increases (three iterations are shown in each panel of Fig. 4), which stems from the periodic dependence on the groove length of the overall complex reflection coefficient ρ_{right} of the groove seen as a distributed reflector. Equation (10) shows that the period, in terms of groove length l, is equal to π/β'_2, *i.e.*, about 0.12 μm. As discussed above, for all intents and purposes, it is in any case better to retain the lowest possible value of l for a given set of the other parameters, in order to limit, and be able to neglect, the losses in the groove.

Comparing Fig. 4(a), 4(b), and 4(c) shows that as L increases, the intervals of ω and l that satisfy the generation condition expressed by Eq. (12) expand, as graphically evidenced by the increasing area of the colour plot. For large values of L, the periodically repeated generation domains can even tend to merge near ω_m (Fig. 4(c)). Comparing the colour gradient of the plots in Fig. 4(a), 4(b), and 4(c) also shows that an increase of the active region length L expands the range of values of d_2/d_1 (in essence, the depth of the groove) suitable for SPP generation. This is due to the fact that with an increase in the effective SPP amplification factor $(\alpha - 2|\beta''_1|)L$ in the resonator, the generation condition can be fulfilled even for a distributed reflector (such as the groove) with a lower reflectivity (for which the amplitude reflection coefficient $|\rho_{right}|$ is significantly<1), which in turn, leads to wider ranges for the parameters l and d_2/d_1 that define the geometry of the groove.

Equation (12) thus predicts that the SPP generation frequency in the structure under study strongly depends on the geometrical parameters of both the groove region and the active waveguide. The choice of the film thickness d_1 common to both waveguides is determined by the synchronization condition between the phase velocity of the SPP and the drift velocity of the pump current so that amplification can actually take place, but the structure can be adjusted to a predetermined working frequency (within the admissible range discussed above) by selecting the length and the depth of the groove, as well as the length of the active waveguide. If the length of the active region is fixed (for example, due to fabrication limitations), different generation frequencies can be obtained for different lengths and/or depths of the groove.

4. Conclusions

In this study, a graphene-based active plasmonic planar waveguide has been proposed for a highly efficient current-driven resonant amplification of slow surface plasmon polaritons. This takes place in a semiconductor waveguide where surface plasmon polaritons are amplified *via* energy exchange with a direct electric current flowing in a graphene layer separating the film from a dielectric substrate. Amplified plasmon polaritons are then extracted towards a passive waveguide connected to the active region through a narrow and shallow groove that also provides the necessary feedback that makes the active waveguide a resonant amplifier.

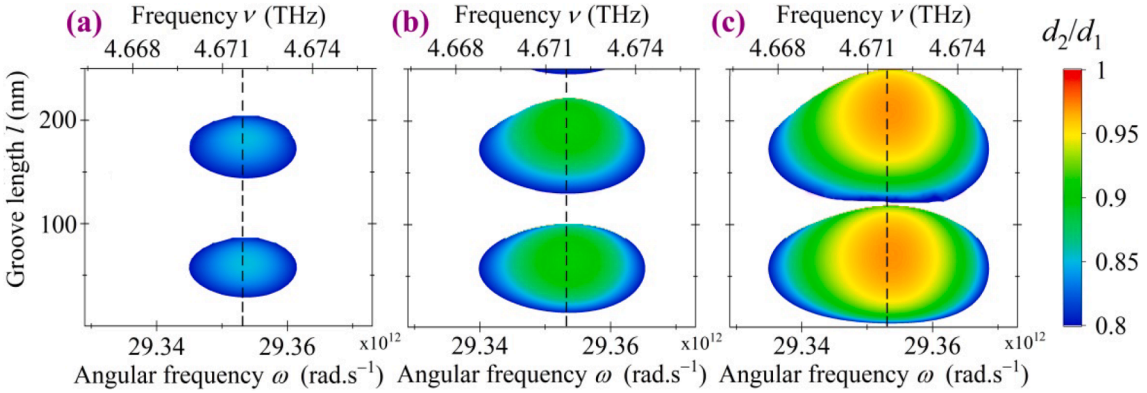

Fig. 4. Ratio d_2/d_1 calculated as a function of the generation frequency and the length l of the groove by numerically solving Eq. (12) for waveguide thickness $d_1 = 50$ nm and for the length of the active waveguide taken as (a) $L = 15$ μm, (b) $L = 20$ μm, and (c) $L = 30$ μm. The vertical black dashed line shows the angular frequency $\omega_m = 29.353 \cdot 10^{12}$ rad·s^{-1}.

Amplification requires that a synchronism condition between the polaritons and the direct electric current be verified. We show that the frequency range and the efficiency of the amplification mechanism are determined by the geometric parameters of the entire complex structure, in particular those of the groove. A great advantage of the scheme is that the structure consists of a single semiconductor film common to the active waveguide, the groove, and the adjacent passive waveguide, and that both resonant amplification and radiation extraction are realized directly in that film. Note that the amplification frequency range can be further extended by using a passive waveguide with a thickness different from that of the active waveguide. It should also be noted that a similar plasmon amplifier could be implemented using a ridge instead of a groove between the waveguides.

The current-driven integrated amplification scheme described in our study can be of particular interest for the design and implementation of coherent surface plasmon polariton emitters, *i.e.*, spasers. In practice, the surface plasmon polaritons can be excited by conventional methods using either photon tunneling in the total internal reflection geometry (in the Kretschmann or Otto configurations) or diffraction effects [60], and be resonantly amplified in the active region. Such current-pumped spasers can be expected to find applications for the next generation of chip-scale optoelectronic and photonic circuits.

Funding

The analytical and numerical simulations of the synchronism condition for resonant electric-current-driven amplification of the SPPs in a planar resonator have been supported by the Ministry of Science and Higher Education of the Russian Federation (projects FEUF-2023-0003 and 075-15-2021-581, respectively). The elaboration of the principle of a novel SPP extraction method and the numerical study of the characteristic parameters of a planar waveguide with a groove defect have been supported by the Russian Science Foundation (project 23-79-30017). Y. D. acknowledges the support from École Nationale d'Ingénieurs de Brest, France and Collège de France (programme PAUSE).

CRediT authorship contribution statement

I.O. Zolotovskii: Conceptualization, Data curation, Investigation, Writing – original draft. **Y.S. Dadoenkova:** Conceptualization, Data curation, Visualization, Writing – original draft, Writing – review & editing. **F.F.L. Bentivegna:** Investigation, Writing – original draft, Writing – review & editing. **A.S. Kadochkin:** Formal analysis. **S.G. Moiseev:** Conceptualization, Investigation, Writing – original draft, Writing – review & editing. **V.V. Svetukhin:** Formal analysis.

Declaration of Competing Interest

The authors declare that they have no known competing financial interests or personal relationships that could have appeared to influence the work reported in this paper.

References

[1] S.I. Azzam, A.V. Kildishev, R.-M. Ma, C.-Z. Ning, R. Oulton, V.M. Shalaev, M. I. Stockman, J.-L. Xu, X. Zhang, Ten years of spasers and plasmonic nanolasers, Light Sci. Appl. 9 (2020) 90.
[2] X. Luo, T. Qiu, W. Lu, Z. Ni, Plasmons in graphene: Recent progress and applications, Mater. Sci. Eng. R: Rep. 74 (2013) 351–376.
[3] Q. Bao, K.P. Loh, Graphene photonics, plasmonics, and broadband optoelectronic devices, ACS Nano 6 (2012) 3677–3694.
[4] S. Kasani, K. Curtin, N. Wu, A review of 2D and 3D plasmonic nanostructure array patterns: fabrication, light management and sensing applications, Nanophotonics 8 (2019) 2065–2089.
[5] F. Monticone, A. Alù, Metamaterial, plasmonic and nanophotonics devices, Rep. Prog. Phys. 80 (2017), 036401.
[6] M. Losurdo, F. Moreno, C. Cobet, M. Modreanu, W. Pernice, Plasmonics: Enabling functionalities with novel materials, J. Appl. Phys. 129 (2021), 220401.
[7] A. Ahmadivand, B. Gerislioglu, Photonic and plasmonic metasensors, Laser Photonics Rev. 16 (2) (2022) 2100328.
[8] Q. Li, X. Wu, Y. Zhou, Plasmonic nanosensors and metasensors based on new physical mechanisms, Chemosensors 10 (2022) 397.
[9] L. Liu, W. Liu, Z. Song, Ultra-broadband terahertz absorber based on a multilayer graphene metamaterial, J. Appl. Phys. 128 (2020), 093104.
[10] Y. Li, R. Paiella, Terahertz radiation processes in critically coupled graphene plasmonic nanostructures, J. Appl. Phys. 128 (2020), 153105.
[11] M.M. Müller, M. Kosik, M. Pelc, G.W. Bryant, A. Ayuela, C. Rockstuhl, K. Słowik, From single-particle-like to interaction-mediated plasmonic resonances in graphene nanoantennas, J. Appl. Phys. 129 (2021), 093103.
[12] A. Kumar, M. Gupta, P. Pitchappa, N. Wang, M. Fujita, R. Singh, Terahertz topological photonic integrated circuits for 6G and beyond: A Perspective, J. Appl. Phys. 132 (14) (2022) 140901.
[13] A. Ahmadivand, B. Gerislioglu, R. Ahuja, Y. Kumar Mishra, Terahertz plasmonics: The rise of toroidal metadevices towards immunobiosensings, Mater. Today 32 (2020) 108.
[14] Y. Fang, M. Sun, Nanoplasmonic waveguides: Towards applications in integrated nanophotonic circuits, Light Sci. Appl. 4 (6) (2015) e294.
[15] G.A. Plotz, H.J. Simon, J.M. Tucciarone, Enhanced total reflection with surface plasmons, J. Opt. Soc. Am. 69 (1979) 419–421.
[16] A.N. Sudarkin, P.A. Demkovich, Excitation of surface electromagnetic waves on the boundary of a metal with an amplifying medium, Sov. Phys. Uspekhi 34 (1989) 764–766.
[17] P. Berini, I. De Leon, Surface plasmon-polariton amplifiers and lasers, Nat. Photon. 6 (1) (2012) 16–24.
[18] M.C. Gather, K. Meerholz, N. Danz, K. Leosson, Net optical gain in a plasmonic waveguide embedded in a fluorescent polymer, Nat. Photonics 4 (2010) 457–461.
[19] D.Y. Fedyanin, A.V. Krasavin, A.V. Arsenin, A.V. Zayats, Surface plasmon polariton amplification upon electrical injection in highly integrated plasmonic circuits, Nano Lett. 12 (2012) 2459–2463.
[20] T. Wijesinghe, M. Premaratne, G.P. Agrawal, Electrically pumped hybrid plasmonic waveguide, Opt. Express 22 (2014) 2681–2694.
[21] V. Ryzhii, M. Ryzhii, T. Otsuji, Negative dynamic conductivity of graphene with optical pumping, J. Appl. Phys. 101 (2007), 083114.
[22] D. Svintsov, T. Otsuji, V. Mitin, M.S. Shur, V. Ryzhii, Negative terahertz conductivity in disordered graphene bilayers with population inversion, Appl. Phys. Lett. 106 (2015), 113501.
[23] A.A. Dubinov, V.Y. Aleshkin, M. Ryzhii, T. Otsuji, V. Ryzhii, Terahertz laser with optically pumped graphene layers and fabri–perot resonator, Applied Physics Express 2 (2009), 092301.
[24] V. Ryzhii, A.A. Dubinov, T. Otsuji, V. Mitin, M.S. Shur, Terahertz lasers based on optically pumped multiple graphene structures with slot-line and dielectric waveguides, J. Appl. Phys. 107 (2010), 054505.
[25] M.Y. Morozov, I.M. Moiseenko, V.V. Popov, Amplification of plasma waves in shielded active graphene, Technical Physics Letters 42 (2016) 40–42.
[26] Y.S. Dadoenkova, S.G. Moiseev, A.S. Abramov, A.S. Kadochkin, A.A. Fotiadi, I. O. Zolotovskii, Surface plasmon polariton amplification in semiconductor–graphene–dielectric structure, Ann. Phys. (Berlin) 529 (2017) 1700037.
[27] I.O. Zolotovskii, Y.S. Dadoenkova, S.G. Moiseev, A.S. Kadochkin, V.V. Svetukhin, A.A. Fotiadi, Plasmon polariton distributed feedback laser with pump by fast drift current in graphene, Phys. Rev. A 97 (2018), 053828.
[28] S.G. Moiseev, Y.S. Dadoenkova, A.S. Kadochkin, A.A. Fotiadi, V.V. Svetukhin, I. O. Zolotovskii, Generation of slow surface plasmon polaritons in a complex waveguide structure with electric current pump, Ann. Phys. (Berlin) 530 (2018) 1800197.
[29] D. Svintsov, Emission of plasmons by drifting Dirac electrons: A hallmark of hydrodynamic transport, Phys. Rev. B 100 (2019), 195428.
[30] T. A. Morgado, M. G. Silveirinha, Negative Landau damping in bilayer graphene. Phys. Rev. Lett. 119 (2017) 133901. See also D. Svintsov, V. Ryzhii, Comment on "Negative Landau damping in bilayer grapheme". Phys. Rev. Lett. 123 (2019) 219401, and T. A. Morgado, M. G. Silveirinha, Morgado and Silveirinha Reply. Phys. Rev. Lett. 123 (2019) 219402.
[31] T.A. Morgado, M.G. Silveirinha, Active graphene plasmonics with a drift-current bias, ACS Photonics 8 (2021) 1129–1136.
[32] S.E. Tsimring (Ed.), Electron Beams and Microwave Vacuum Electronics, Wiley, 2006.
[33] P.A.D. Gonçalves, N.M.R. Peres, An introduction to graphene plasmonics, World Scientific, Singapore, 2016.
[34] R. Kitamura, L. Pilon, M. Jonasz, Optical constants of silica glass from extreme ultraviolet to far infrared at near room temperature, Appl. Opt. 46 (2007) 8118–8133.
[35] S. Adachi, GaAs and Related Materials, Bulk Semiconducting and Superlattice Properties, World Scientific, Singapore, 1994.
[36] G.W. Hanson, Dyadic Green's functions and guided surface waves for a surface conductivity model of graphene, J. Appl. Phys. 103 (2008), 064302.
[37] M.A. Yamoah, W. Yang, E. Pop, D. Goldhaber-Gordon, High-velocity saturation in graphene encapsulated by hexagonal boron nitride, ACS Nano 11 (2017) 9914–9919.
[38] H. Ramamoorthy, R. Somphonsane, J. Radice, G. He, C.P. Kwan, J.P. Bird, "Freeing" graphene from its substrate: observing intrinsic velocity saturation with rapid electrical pulsing, Nano Lett. 16 (2016) 399–403.
[39] M.D. Ozdemir, O. Atasever, B. Ozdemir, Z. Yarar, M. Ozdemir, A comparative study of transport properties of monolayer graphene and AlGaN-GaN heterostructure, AIP Adv. 5 (2015), 077101.

[40] K.S. Novoselov, A.K. Geim, S.V. Morozov, D. Jiang, M.I. Katsnelson, I. V. Grigorieva, S.V. Dubonos, A.A. Firsov, Two-dimensional gas of massless Dirac fermions in graphene, Nature 438 (2005) 197–200.
[41] B. Dastmalchi, P. Tassin, T. Koschny, C.M. Soukoulis, A new perspective on plasmonics: Confinement and propagation length of surface plasmons for different materials and geometries, Adv. Opt. Mater. 4 (2016) 177–184.
[42] R. Soref, R.E. Peale, W. Buchwald, Longwave plasmonics on doped silicon and silicides, Opt. Express 16 (2008) 6507–6514.
[43] C. Hwang, D.A. Siegel, S.-K. Mo, W. Regan, A. Ismach, Y. Zhang, A. Zettl, A. Lanzara, Fermi velocity engineering in graphene by substrate modification, Sci. Rep. 2 (2012) 590.
[44] P.V. Ratnikov, A.P. Silin, Novel type of superlattices based on gapless graphene with the alternating Fermi velocity, JETP Lett. 100 (2014) 311–318.
[45] A. Yariv, Quantum Electronics, Wiley, New York, 1989.
[46] R.F. Oulton, D.F.P. Pile, Y. Liu, X. Zhang, Scattering of surface plasmon polaritons at abrupt surface interfaces: Implications for nanoscale cavities, Phys. Rev. B 76 (2007), 035408.
[47] A.Y. Nikitin, F. López-Tejeira, L. Martín-Moreno, Scattering of surface plasmon polaritons by one-dimensional inhomogeneities, Phys. Rev. B 75 (2007), 035129.
[48] J.L. Garcia-Pomar, A.Y. Nikitin, L. Martin-Moreno, Scattering of graphene plasmons by defects in the graphene sheet, ACS Nano 7 (2013) 4988–4994.
[49] A.J. Chaves, B. Amorim, Y.V. Bludov, P.A.D. Gonçalves, N.M.R. Peres, Scattering of graphene plasmons at abrupt interfaces: An analytic and numeric study, Phys. Rev. B 97 (2018), 035434.
[50] F. Guan, S. Sun, S. Ma, Z. Fang, B. Zhu, X. Li, Q. He, S. Xiao, L. Zhou, Transmission/reflection behaviors of surface plasmons at an interface between two plasmonic systems, J. Phys.: Condens. Matter 30 (11) (2018) 114002.
[51] J. Ctyroky, J. Petracek, V. Kuzmiak, P. Kwiecien, I. Richter, Silicon waveguides with graphene: coupling of waveguide mode to surface plasmons, J. Opt. 22 (2020), 095801.
[52] G.I. Stegeman, N.E. Glass, A.A. Maradudin, T.P. Shen, R.F. Wallis, Fresnel relations for surface polaritons at interfaces, Opt. Lett. 8 (1983) 626–628.
[53] E.A. Bezus, L.L. Doskolovich, N.L. Kazanskiy, Low-scattering surface plasmon refraction with isotropic materials, Opt. Express 22 (2014) 13547–13554.
[54] I. Friedler, P. Lalanne, J.P. Hugonin, J. Claudon, J.M. Gérard, A. Beveratos, I. Robert-Philip, Efficient photonic mirrors for semiconductor nanowires, Opt. Lett. 33 (2008) 2635–2637.
[55] R. Gordon, Light in a subwavelength slit in a metal: Propagation and reflection, Phys. Rev. B 73 (2006), 153405.
[56] A.Y. Nikitin, T. Low, L. Martin-Moreno, Anomalous reflection phase of graphene plasmons and its influence on resonators, Phys. Rev. B 90 (2014) 041407(R).
[57] J.-H. Kang, S. Wang, Z. Shi, W. Zhao, E. Yablonovitch, F. Wang, Goos-Hänchen shift and even-odd peak oscillations in edge reflections of surface polaritons in atomically thin crystals, Nano Lett. 17 (2017) 1768–1774.
[58] S. Wang, F. Wu, K. Watanabe, T. Taniguchi, C. Zhou, F. Wang, Metallic Carbon Nanotube Nanocavities as Ultracompact and Low-loss Fabry-Perot Plasmonic Resonators, Nano Lett. 20 (2020) 2695–2702.
[59] X. Luo, C. Hu, B. Lyu, L. Yang, X. Zhou, A. Deng, J.-H. Kang, Z. Shi, Reflection phase shift of one-dimensional plasmon polaritons in carbon nanotubes, Phys. Rev. B 101 (2020) 041407(R).
[60] A.V. Zayats, I.I. Smolyaninov, Near-field photonics: surface plasmon polaritons and localized surface plasmons, J. Opt. A: Pure Appl. Opt. 5 (4) (2003) S16–S50.